Design of Wideband Fractal MIMO Antenna using Minkowski and Koch Hybrid Curves on Half Octagonal Radiating Patch with High Isolation and Gain for 5G Applications

Amandeep Kaur Sidhu[1] and Jagtar Singh Sivia[2]
[1]Department of Electronics Communication Engineering, Punjabi University, Patiala, Punjab, India
[2]Yadavindra Department of Engineering Punjabi University Guru Kashi Campus Talwandi Sabo, Bathinda, Punjab, India

Corresponding author: Amandeep Kaur Sidhu (e-mail: sidhu. amandeep23@gmail. com).

ABSTRACT This article represents a Multiple Input Multiple Output (MIMO) hybrid fractal antenna with a wider bandwidth. The hybrid fractal MIMO antenna is created by integrating Minkowski and Koch curves on a half octagonal radiating patch. A wider impedance bandwidth 20. 4GHz (1. 0 to 21. 4GHz) and 6. 10GHz (23. 9 to 30GHz) along with fractional bandwidth of 182. 14% and 22. 63% has been achieved by using an amalgamated fractal configuration and a tapered microstrip feed line. The proposed antenna retains high isolation between -20 to -50dB in the entire frequency range along with a DG value greater than 9. 99 dB, ECC less than 0. 02 and acceptable value of gain. Hence, the proposed hybrid fractal MIMO antenna is a proficient candidate for 5G, 3. 5GHz band (3. 4 – 3. 6GHz), 5G NR (New Radio) frequency bands (3. 3 – 5. 0GHz), LTE band 46 (5. 15 – 5. 925GHz), EU (European Union) 5G frequency band (5. 9 – 6. 4GHz), UWB applications (3. 1 – 10. 6GHz) and 5G 26GHz frequency band.

INDEX TERMS Isolation, Mutual coupling, MIMO, Correlation coefficient, Multiband antenna, Stubs.

I. INTRODUCTION

There is a growing demand for portable/hand-held wireless devices that can transmit or receive audio/video streaming with a high transmission rate and good transmission reliability in today's technological era. To transmit these messages at a fast data rate while maintaining signal quality, a considerable channel capacity is required. The standard Single Input Single Output (SISO) communication system, as Shannon's theorem, is incapable of performing these operations due to its limited channel capacity. To tackle this challenge, different researchers used different methodologies and approaches. After continued attempts to tackle the problem, the Multiple Input Multiple Output (MIMO) communication system was established, which is capable of transferring data at a high rate and reducing signal disappearance in a rich scattering atmosphere with no additional power or spectrum cost. Because of the spatial component that is absent in SISO systems, antennas used in such communications networks are said to be MIMO antennas, capable of fundamentally minimizing the impacts of multipath, and network quantity, causing stronger link consistency, channel capacity, gain, handling without need of extra bandwidth and diversity performance. In MIMO systems, lossless faster data rates are achieved using techniques such as Space-Time Coding (STC) and Spatial Multiplexing. STC aids diversity, while Spatial Multiplexing allows a MIMO transmitter/receiver pair to boost performance without affecting broadcast power or bandwidth utilization. MIMO antennas normally have at least two radiating elements that are separated by some distance and with excellent isolation among them. The amount of space allocated in hand-held/portable wireless front-ends is quite limited, which can lead to mutual coupling and performance distortion. Many methodologies and procedures have been proposed by various researchers to reduce mutual coupling and improve isolation without compromising on performance; introduction of parasitic elements [1-2], use of metamaterials to attain low correlation between antenna elements [3], by loading (Split Ring Resonators) SRRs [4-5], employment of EBG (Electromagnetic Band Gap) structures [6-7], by introducing meandered-line resonator [8], introducing Defected Ground Structure (DGS) [9-13], by employing slots, slits and stubs in the ground structure as well as on the radiating elements [14-15], by incorporation of SRR and EBG structures [16], use of Substrate Integrated Waveguide (SIW) technology [17], employing diamond-shaped patterned ground resonator [18].

The most used fractal geometries which are used in designing the antennas are Giuseppe Peano [19-21], Sierpinski Gasket/Carpet [22-25], Koch [26-28], Minkowski [29-32], Meander [33-35], Hilbert [36-38], stair case[39], etc. Each type of fractal structure has its exceptional inference in the design structure of the antenna for the specific wireless communication standards [40-43]. Sometimes, a single fractal structure is used to design radiating elements unable to reveal the desired characteristics. To solve this, distinct investigators developed the geometries of hybrid fractal antennas (HFA) for different wireless communication standards. The different hybrid fractal antennas are Koch-Meander [44], Sierpinski carpet/gasket-Giuseppe Peano-Koch, Koch-SierpinskiCarpet/gasket, Sierpinski carpet/gasket-Giuseppe Peano Sierpinski carpet-Sierpinski gasket, Giuseppe Peano-Cantor set-Sierpinski Carpet[45], etc.

Other fractal geometries such as Sunflower and Amer fractal are also described by the researchers [46-47]. The various types of fractal geometrical structures are used by the investigators to design the hybrid and fractal antenna which are suitable for 5G communications [48-58]. MIMO antennas are a proficient candidate for integrally justifying the properties of network quantity, and multipath, producing the best-quality dependability of the link, and channel volume, gain exposure without challenging more impedance bandwidth for additional enlightening the quantity and spectrum effectiveness of MIMO antennas. The massive MIMO emanated into presence, somewhat it is a development of MIMO which essentially clusters the antennas together at the receiver/transmitter. Fractal antennas are suitable for creating massive MIMO antennas due to its important properties such as space-filling and self-similarity. Numerous researchers have functioned in this track and designed the Massive MIMO structures of the antenna which is suitable for 5G communications [59-67].

In this paper, Koch and Minkowski geometries are attached together to generate a hybrid fractal curve, and further this curve has been overlaid on a half octagonal shaped patch to design the novel structure of the element of a hybrid MIMO antenna.

II. DESIGN METHODLOGY AND CONFIGURATION

This section reveals the several designing process and investigation of parametric analysis of simulated designed MIMO antenna. In this manuscript, the final prototype of the antenna has been attained by employing the Minkowski and Koch curves on the half octagonal shaped radiating patch with a modified ground plane. The procedure of designing the half octagonal shaped radiating patch, hybridization, and superimposition of Minkowski and Koch fractal curves using IFS (Iterative Function System) on the proposed radiating patch with modified ground plane and its numerous parameters are deliberated in this section. The reason behind introducing the hybrid curve and modified ground structure is to improve the isolation of the MIMO antenna along with other performance parameters which are discussed in detail in the forthcoming sub-sections.

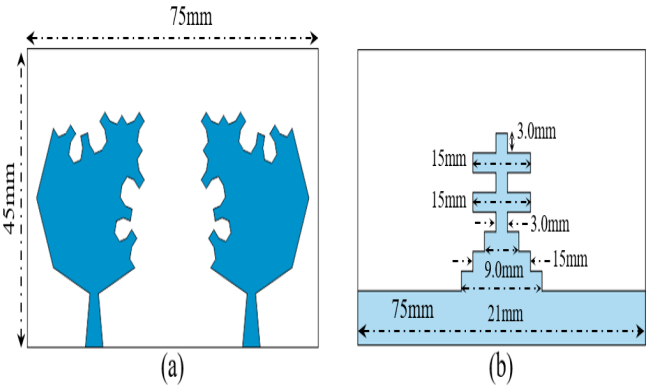

FIGURE 1. Proposed wideband hybrid MIMO (multi-input-multi-output) antenna geometric prototype: (a) front view and (b) rear view.

The proposed 2×2 wideband hybrid MIMO (multiple-input-multiple-output) is printed on Rogers RT/duroid 5880 has been used with a thickness of 1. 6mm with relative permittivity 2. 2, loss tangent 0. 0009, and mass density 0 kg/m^3. The front and rear geometrical prototype of the proposed MIMO antenna is delineated in Fig. 1. The proposed antenna comprises two antenna elements. A modified ground plane has been employed to improve the isolation as well as the other parameters of the designed antenna as delineated in Fig. 1 (a). The patch and the modified ground structure are made up of copper with stable conductivity of 5. 8 × 10^7 S/m. The structures of the MIMO antenna are simulated using the HFSS V13 simulator and the antenna occupies an area of 45mm × 75mm. The parametric dimensions of the proposed MIMO antenna are depicted in Fig. 1 and Fig. 2.

A. DESIGN AND ANALYSIS OF SINGLE ELEMENT OF ANTENNA

$$R = \frac{F}{\left\{1 + \frac{2h}{\pi F \varepsilon_r}\left[\ln\left(\frac{\pi F}{2h}\right) + 1.7726\right]\right\}^{\frac{1}{2}}} \quad (1)$$

Where;

$$F = \frac{8.791 \times 10^9}{f_r \sqrt{\varepsilon_r}}$$

The proposed antenna initiates with the designing of the octagonal shaped patch and its radius is assessed with the help of equation (1), by using various designing parameters. The radius of the octagonal radiating patch (R) has been calculated and found to be 14. 85mm with a resonant frequency of 2. 25GHz. After this patch has been excited by

using a 50Ω transmission feed line and the partial ground plane with length 'G2' has been used in the initial geometry for better impedance matching throughout the desired frequency range as delineated in Fig. 2(a); named as a step–1. In the next step (step – 2) the transmission line has been made tapered for improving the impedance matching in relation with the reflection coefficient as illustrated in Fig. 2(b). To improve the performance of the antenna further in terms of impedance matching, the half octagonal patch has been etched from antenna elements to acquire the desired structure of the patch as shown in Fig. 2(c) and designated as a step – 3.

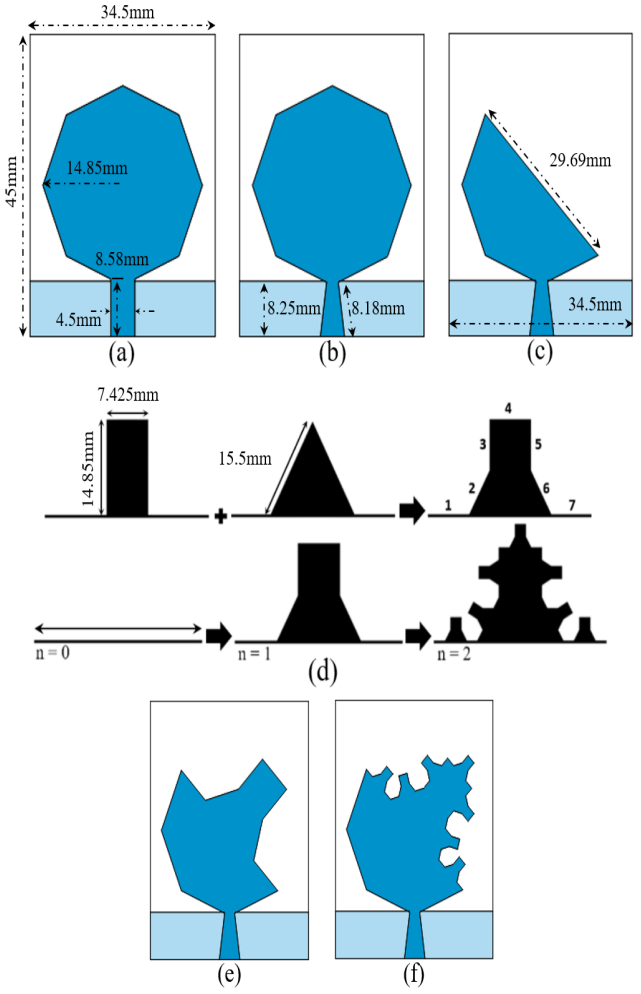

FIGURE 2. Process of designing the single element of proposed MIMO hybrid antenna (a) step – 1, (b) step – 2, (c) step – 3, (d) hybridization of Minkowski and Koch fractal curves, (e) step – 4 and (f) step – 5 (proposed antenna element).

The progression of the various design steps of a single element of the designed MIMO antenna has been discussed and illustrated in Fig. 2. The design process comprises five different types of antennas from step – 1 to step – 5. The final geometry (proposed unit element) of the antenna is shown in Fig. 2(f); which is used for the dual element (2×2) MIMO antenna.

The S-parameters (S_{11}) in terms of reflection coefficient at -10dB reference for the initial three steps (step – 1 to step –3) are delineated in Fig. 3. It can be clearly observed from Fig. 3, that at the first step (step – 1) antenna radiates, at 4. 5, 18. 7 and 26. 6GHz frequency bands with a corresponding reflection coefficient of -23. 07, -14. 0, and -22. 48GHz. It also exhibits the wideband response from 2. 45 – 12. 0GHz, 13. 6-22. 4 GHz, and 24. 0 – 29. 7GHz. Thus, in step -2, the tapered feed line has been introduced and the antenna shows the enhanced bandwidth from 2. 30 – 22. 30GHz and 24. 0 – 30. 0GHz as compared to the previous step and also exhibits the additional frequency band with an improved reflection coefficient of -37. 0dB. To enhance the performance of the designed antenna further, step – 3 with half octagonal shaped radiating patch with a tapered feed line has been designed which shows the improvement in the reflection coefficient (-43. 22dB) at the 20. 0GHz frequency band without altering the bandwidth of the antenna as compared to the antenna designed in the previous step. From, the above discussion it is clear that by modifying the geometry of the antenna, the impedance bandwidth as well as the reflection coefficient gets improved. The main goal of this work is to design the antenna element with wider bandwidth from 1 to 30GHz frequency range. So, to attain the desired impedance matching characteristics the further steps (step – 4 and step–5) of the antenna have been designed by superimposing the Minkowski and Koch curves up to the 2nd iteration on a half octagonal patch designed in (step -3).

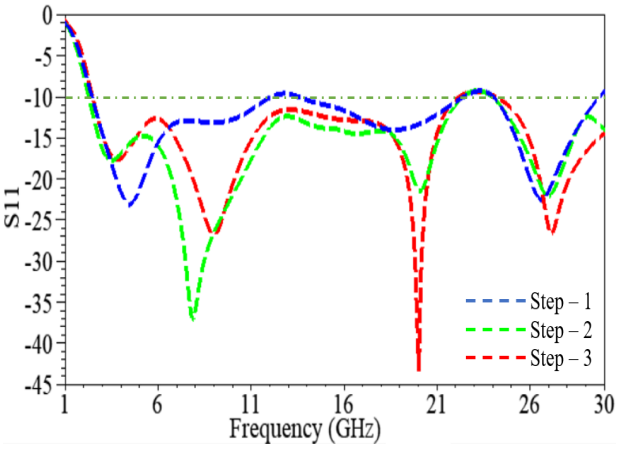

FIGURE 3. Comparison of S_{11} versus frequency plot of various geometrical steps of proposed single element.

The versatile mathematical tool called IFS has been used to design the required hybrid curve as shown in Fig. 2 (d). An Iteration function system (IFS) is a mathematical technique for designing fractal geometry that creates a generator curve. The subsequent iterations of the fractal antenna are easily obtained. In this design, two types of fractal curves are fused together such as Minkowski fractal curve with indentation angle θ = 90° and the Koch fractal curve with angle θ = 60° depicted in Fig. 2(d) and designated as the generator curve. This generator can be used as the base geometry to obtain the

next iterations of a similar shape. The generator curve comprises seven segments. For achieving the required fractal curve, the design process has been started with a straight line, called an initiator with n = 0 and a generator curve with n = 1. The length of the initiator (straight line) is equal to the diagonal cut of the half octagonal shaped radiating patch (H_1 = 29. 69mm). The same procedure is repetitive up to the 2nd iteration with n = 2. The final geometry has been obtained by duplication of the reduced form of the generator curve on the seven segments of the generator itself. Due to the self-similarity property, the total length '*l*' of the final curve is given by [68-69]:

$$l = h\left(\frac{N}{r}\right)^{n} = 29.69\left(\frac{7}{4}\right)^{2} = 90.925mm \qquad (2)$$

Here 'r' represents the sum of individual segments alienated on iteration, 'N' denotes the number of sections, 'n' specifies the number of iterations and 'h' represents the height of the curve.

IFS is used to achieve the above-mentioned geometry of a hybrid fractal curve by smearing affine transformations *(T)* to an elementary shape *(E)*. Affine conversion contains scaling, transformation and rotation and can be represented as:

$$T(x) = Ex + t = \begin{bmatrix} a & b \\ c & d \end{bmatrix}\begin{bmatrix} x_1 \\ x_2 \end{bmatrix}\begin{bmatrix} e \\ f \end{bmatrix} \qquad (3)$$

Where matrix *E* (initial structure) is given as:

$$E = \begin{bmatrix} \left(\frac{1}{s}\right)\mathrm{Cos}\,\theta & -\left(\frac{1}{s}\right)\mathrm{Sin}\,\theta \\ \left(\frac{1}{s}\right)\mathrm{Sin}\,\theta & \left(\frac{1}{s}\right)\mathrm{Cos}\,\theta \end{bmatrix} \qquad (4)$$

Here 'a to d' are used for scaling and rotation, 'e and f' are used for the conversion and shifting, 's' is the scaling factor, 'θ' is the rotation angle, 't' characterizes the transformation factor, and 'x_1, x_2' indicates the coordinate points of x.

By using the set of linear transformations on '*E*' and using the Hutchinson operator (*T*), the desired hybrid fractal curve can be attained by using the succeeding equation [70]:

$$T(E) = \bigcup_{n=1}^{N} K_N(Z) \qquad (5)$$

Conversion of each segment to produce the anticipated structure of fractal curve as described in Fig. 2(d) can be attained by using aforementioned operator (*T*) and represented as:

$$T_1\begin{bmatrix} x_1 \\ x_2 \end{bmatrix} = \begin{bmatrix} 0.200 & 0 \\ 0 & 0.200 \end{bmatrix}\begin{bmatrix} x_1 \\ x_2 \end{bmatrix} + \begin{bmatrix} 0 \\ 0 \end{bmatrix} \qquad (6)$$

$$T_2\begin{bmatrix} x_1 \\ x_2 \end{bmatrix} = \begin{bmatrix} 0.200 & -0.250 \\ 0.250 & 0.200 \end{bmatrix}\begin{bmatrix} x_1 \\ x_2 \end{bmatrix} + \begin{bmatrix} 0.200 \\ 0 \end{bmatrix} \qquad (7)$$

$$T_3\begin{bmatrix} x_1 \\ x_2 \end{bmatrix} = \begin{bmatrix} 0 & -0.250 \\ 0.250 & 0 \end{bmatrix}\begin{bmatrix} x_1 \\ x_2 \end{bmatrix} + \begin{bmatrix} 0.400 \\ 0.250 \end{bmatrix} \qquad (8)$$

$$T_4\begin{bmatrix} x_1 \\ x_2 \end{bmatrix} = \begin{bmatrix} 0.200 & 0 \\ 0 & 0.200 \end{bmatrix}\begin{bmatrix} x_1 \\ x_2 \end{bmatrix} + \begin{bmatrix} 0.400 \\ 0.250 \end{bmatrix} \qquad (9)$$

$$T_5\begin{bmatrix} x_1 \\ x_2 \end{bmatrix} = \begin{bmatrix} 0 & 0.250 \\ -0.250 & 0 \end{bmatrix}\begin{bmatrix} x_1 \\ x_2 \end{bmatrix} + \begin{bmatrix} 0.600 \\ 0.500 \end{bmatrix} \qquad (10)$$

$$T_6\begin{bmatrix} x_1 \\ x_2 \end{bmatrix} = \begin{bmatrix} 0.200 & 0.250 \\ -0.250 & 0.200 \end{bmatrix}\begin{bmatrix} x_1 \\ x_2 \end{bmatrix} + \begin{bmatrix} 0.600 \\ 0.250 \end{bmatrix} \qquad (11)$$

$$T_7\begin{bmatrix} x_1 \\ x_2 \end{bmatrix} = \begin{bmatrix} 0.200 & 0 \\ 0 & 0.200 \end{bmatrix}\begin{bmatrix} x_1 \\ x_2 \end{bmatrix} + \begin{bmatrix} 0.800 \\ 0 \end{bmatrix} \qquad (12)$$

Where T_1, T_2, T_3, T_4, T_5, T_6, and T_7 are the set of a linear transformation, and the originator curve is then achieved by using $T(E) = T_1(E) \cup T_2(E) \cup T_3(E) \cup T_4(E) \cup T_5(E) \cup T_6(E) \cup T_7(E)$. This method can be repetitive for gaining further repetitions of the anticipated hybrid fractal curve, for the self-similarity index (D), deliberate by using the following equation:

$$D = \frac{\log(N)}{\log(r)} = \frac{\log(7)}{\log(4)} = 1.4036 \qquad (13)$$

The Koch and Minkowski curves are designed and merged together to attain desired hybrid fractal curve. Further, this designed hybrid curve (1st iteration (n=1) and 2nd iteration (n=2)) is integrated with the half octagonal shaped radiating patch as exemplified in Fig. 2(e) and Fig. 2(f) respectively. The 2nd iteration (n=2) of the hybrid curve on half octagonal shaped radiating patch as shown in Fig. 2(f) is designated as the final geometry of a single component of the proposed MIMO antenna.

The comparison of the reflection coefficient of step – 4 and step – 5 is illustrated in Fig. 4. It is observed from Fig. 4, that antenna designed in step – 4 by applying the 1st iteration of hybrid fractal radiates in frequency ranges of 2. 3–21. 68GHz and 23. 4–30. 0GHz with corresponding bandwidth of 19. 38GHz and 6. 6GHz.

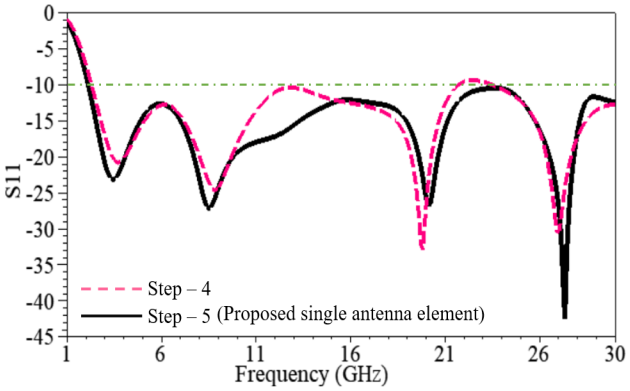

FIGURE 4. Comparison of S_{11} versus frequency plot of last two (step – 4 and 5) geometrical steps of proposed single element.

Finally, the antenna designed in step – 5 exhibits wider bandwidth of 27. 87GHz (2. 13 – 30GHz) with an enhanced reflection coefficient of -23. 16, -27. 19, 26. 86, and -42. 48dB at the corresponding frequency bands of 3. 5, 8. 5, 20. 1, and 27. 3GHz respectively. It is apparent from the comparison of simulated S-parameters (S_{11}) of the antenna designed from step – 1 to step – 5, that the single element of the antenna reveals the improvement in the impedance characteristics in relation with bandwidth and reflection coefficient by modifying the geometry of radiating patch. The final structure of the designed hybrid single antenna element (step–5) is fabricated and tested for the authentication of the result. So, the comparison of simulated and measured S_{11} parameters of single element antenna along with the fabricated prototype is demonstrated in Fig. 5 which shows good agreement between the results. However, there are some variations between both the results, which are due to the losses from the connector wires during testing on VNA, reflection from SMA connector, soldering bumps, environmental conditions, vagueness in electric properties of the substrate, etc. Further, the designed structure of the antenna can be enhanced by designing the dual element MIMO antenna based on the proposed structure attained in step -5.

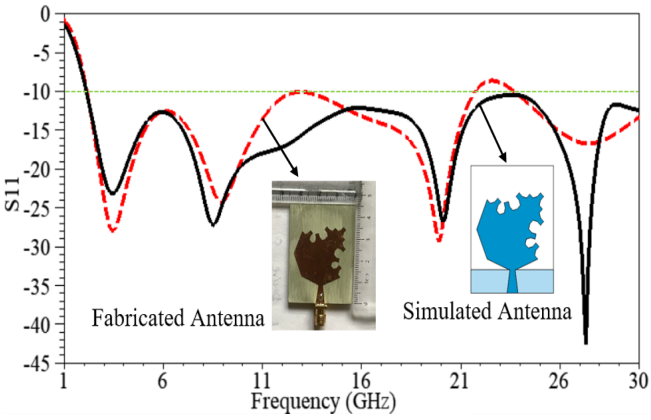

FIGURE 5. Comparison of simulated and measured S_{11} parameter of single element antenna.

III. TWO PORT MIMO ANTENNA DESIGN AND ANALYSIS

In this segment, the design of the two-port MIMO structure of the antenna has been obtained by using two, single hybrid antenna radiating elements designed in the previous section. The MIMO antenna radiating elements are arranged in a way that the second element is the mirror image of the first element as illustrated in Fig. 6. Initially, the simple ground plane is used in the geometry of the MIMO antenna as delineated in Fig. 6(a). To improve the performance of the MIMO antenna the simple ground plane has been modified by applying staircase geometry along with stubs as illustrated in Fig. 6(b). The comparison of S-parameters (S_{11}/S_{22} reflection coefficient) and S_{12}/S_{21} (isolation characteristics) for both configurations of the antenna with and without modified ground plane have been portrayed in Fig. 7.

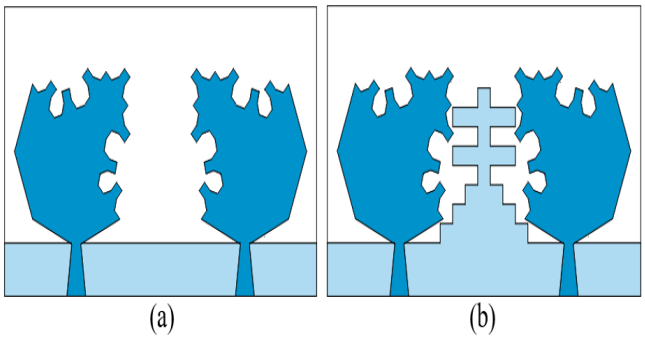

FIGURE 6. Proposed 2×2 wideband hybrid MIMO (multi-input-multi-output) antenna: (a) simple ground plane and (b) modified ground plane.

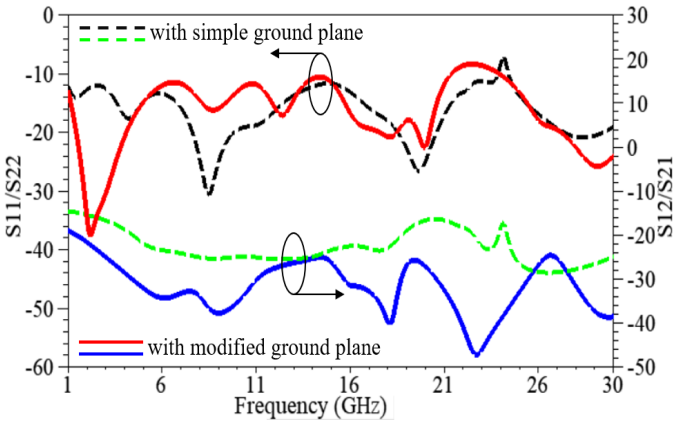

FIGURE 7. Comparison of reflection coefficient and isolation versus frequency plot of different configuration of proposed MIMO antenna.

It can be anticipated from Fig. 7, that the MIMO antenna with a simple ground plane resonates at the frequency spectrum of 1. 0 to 23. 87GHz and 24. 41 to 30. 0GHz with corresponding impedance bandwidth of 22. 87GHz and 5. 59GHz and maintain the isolation (S_{21}) of -15dB to -20dB between the frequency range of 1. 0 to 4. 5GHz, similarly the isolation is between -15dB to -26dB up to the frequency of

18. 75GHz and for rest of the frequency range the isolation is fluctuating between -16dB to -29dB. The main motive to design the proposed MIMO antenna is to attain isolation below -25dB for the desired frequency range. So, to improve the isolation as well as the reflection coefficient and condense the mutual coupling among the antenna elements the ground plane of the proposed MIMO antenna has been modified. It has been clearly observed from Fig. 7 that due to the amendment in the ground plane the reflection coefficient has been improved from -12. 41dB to -37. 75dB at 2. 2GHz frequency; also the mutual coupling among the elements has been condensed and reveals the isolation below -25dB for the entire frequency range from 1 to 30GHz. Further, the effects of the modification in the ground plane on the performance of the designed MIMO antenna have also been observed and explained in detail in the upcoming sub-section.

A. EFFECTS OF MODIFICATION IN GROUND PLANE

This sub-section presents the parametric analysis of different modified stages of the ground plane of the proposed MIMO antenna. Four distinct types of modification in the ground plane are introduced to accomplish the desired improved performance parameters such as isolation and reflection coefficient. Progress of the modified ground plane from Type-1 to Type-4 (proposed) is illustrated in Fig. 8. Whereas, the dimensions of each element of the modified ground plane are already shown in the previous section (section 2) in Fig. 1.

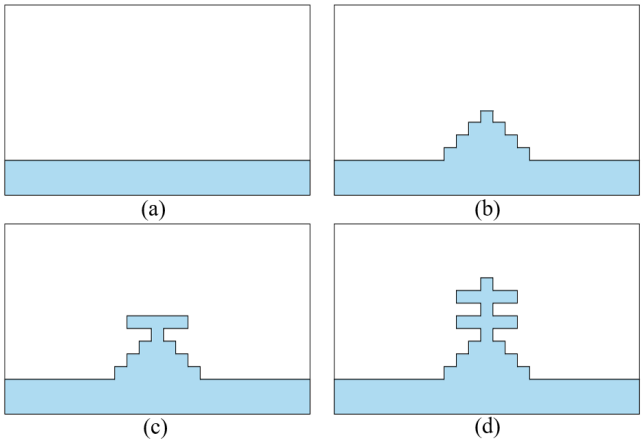

FIGURE 8. Progress of modified ground plane: (a) Type – 1, (b) Type – 2, (c) Type – 3 and (d) Type – 4 (proposed).

The comparison of the reflection coefficient (S_{11}/S_{22}) and isolation (S_{21}/S_{12}) of all four types of the ground plane are delineated in Fig. 9 and Fig. 10 respectively. It can be contemplated from these figures that, simple ground plane/partial ground plane (Type-1) exhibits a bandwidth of 22. 87GHz and 5. 59GHz but the isolation is fluctuating between -14 to -30dB. As, the antenna with a Type-1 ground plane exhibits proper impedance matching over a wide frequency range, but it does not expand the isolation among the antenna elements. Further, to improve the isolation as well as impedance matching characteristics, the staircase geometry is employed on the partial ground plane to generate the structure as shown in Fig. 8(b) also called Type-2. By observing the results of the Type-2 ground plane it has been concluded that the antenna exhibits the two frequency ranges from 4. 6 to 21. 6GHz and 24. 78 to 30. 0GHz with isolation below -25dB.

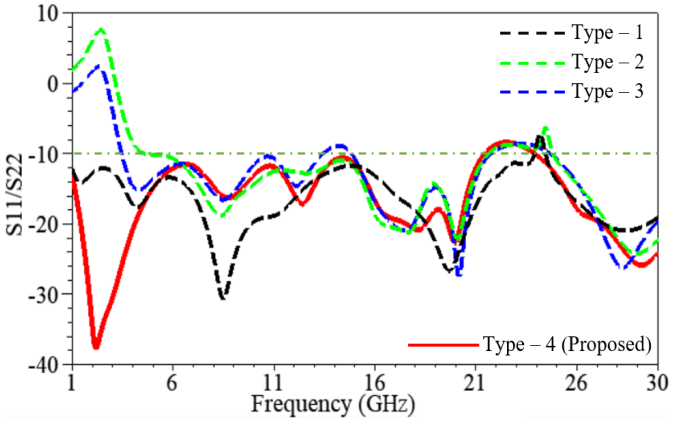

FIGURE 9. Comparison of reflection coefficient versus frequency plot of different types of ground structures of proposed MIMO antenna.

Though the antenna with a Type-2 ground plane exhibits enhanced isolation but it does not radiate below the 4. 6GHz frequency point. Similarly, the T-shaped stub has been introduced on the staircase geometry as shown in Fig. 8(c) termed as Type-3. It can be anticipated that antenna with a Type-3 ground plane degrades the impedance matching characteristics as well as isolation of the proposed MIMO antenna and reveals three frequency ranges from 3. 4 – 13. 42GHz, 14. 83 – 21. 70GHz, and 24. 70 – 30. 0GHz.

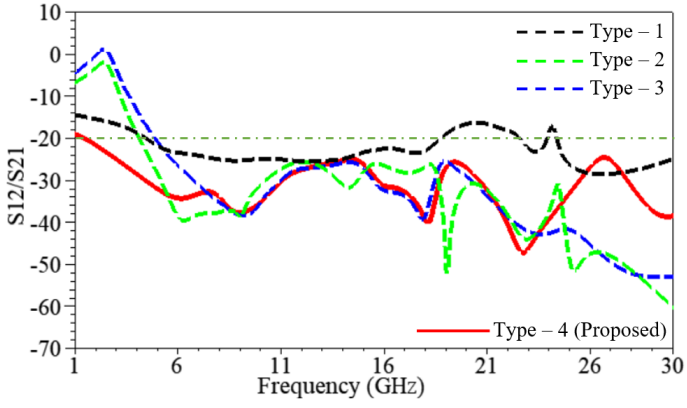

FIGURE 10. Comparison of isolation characteristics plot of different types of ground structures of proposed MIMO antenna.

Finally, to improve the reflection coefficient along with the isolation, the plus '+' shaped stub is employed in the ground plane of the previous geometry (Type-3) to generate a new geometry of the ground plane called Type-4 as shown in Fig. 8(d). By using the Type-4 geometry of the

ground plane; the proposed MIMO antenna radiates in the frequency spectrum from 1. 0 to 21. 4GHz and 23. 9 to 30GHz with corresponding impedance bandwidth of 20. 4GHz and 6. 10GHz respectively. This antenna also reveals the isolation between -25dB to -50dB for the complete frequency range from 1 to 30GHz with a reduction in the mutual coupling among the antenna elements. From, the above discussion it can be predicted that the proposed antenna with Type-4 (proposed) ground plane exhibits better performance in terms of the reflection coefficient and isolation.

B. DIVERSITY PERFORMANCE PARAMETERS OF PROPOSED MIMO HYBRID FRACTAL ANTENNA

Anticipated MIMO antenna distinct diversity parameters like DG (Diversity Gain), ECC (Envelope Correlation Coefficient), TARC (Total Active Reflection Coefficient), and CCL (Channel Capacity Loss) are essential to be investigated and calculated for its effective performance. These performance parameters are analyzed and discussed in detail as follows.

1) ECC

ECC is associated with the radiation pattern, relatively; it advocates how the radiation patterns of two antenna elements are independent of each other. If one element is horizontally polarised then the other will be vertically polarised, then both the antenna elements have zero correlation. Hence, the correlation between the radiation patterns of two elements can be named as the ECC of the MIMO antenna. The preferably required value of ECC is zero, but for practically uncorrelated MIMO antenna satisfactory limits of ECC are less than 0. 5 (ECC<0. 5). The graph of ECC versus frequency for the proposed antenna with a simple and modified ground plane has been evaluated using S-parameters with the help of the following equation. The comparison of ECC of the proposed MIMO antenna for both the configuration of the ground plane is revealed in Fig. 11(a). It can be observed clearly from Fig. 11(a), that the antenna with a modified ground plane exhibits the value of ECC between 0. 01 to 0. 03 for the entire operating frequency range. This value is very much less as compared to the proposed antenna with a simple ground plane [71].

$$ECC = \frac{\left|S_{11}^{*}S_{12} + S_{21}^{*}S_{22}\right|^{2}}{\left(1-\left(\left|S_{11}\right|^{2}+\left|S_{21}\right|^{2}\right)\right)\left(1-\left(\left|S_{22}\right|^{2}+\left|S_{12}\right|^{2}\right)\right)} \quad (14)$$

2) DG

The Diversity Gain (DG) of the MIMO antenna is an important parameter to analyze the performance of the designed antenna. The anticipated value of DG should be approximately 10dB at the operational frequency point, for achieving good quality and consistency in MIMO systems. The diversity gain of the proposed antenna can be premeditated by using the following equation [72].

$$DG = 10 \times \sqrt{1-\left|ECC\right|} \quad (15)$$

According to the equation, the DG of proposed the antenna has been evaluated by using the envelope correlation coefficient. The variation of DG with frequency of the designed MIMO antenna with a simple and modified ground plane has been delineated in Fig. 11(b), from this figure, it can be authenticated that the DG of the proposed antenna is 10dB (approximately) for the complete operational frequency range.

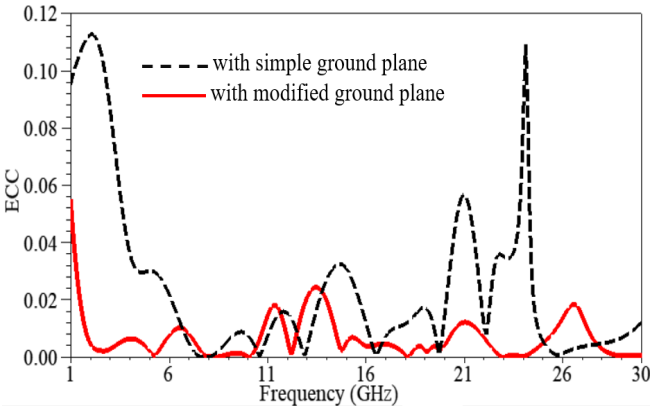

FIGURE 11(a). Envelope correlation coefficient versus frequency plot of proposed MIMO hybrid antenna.

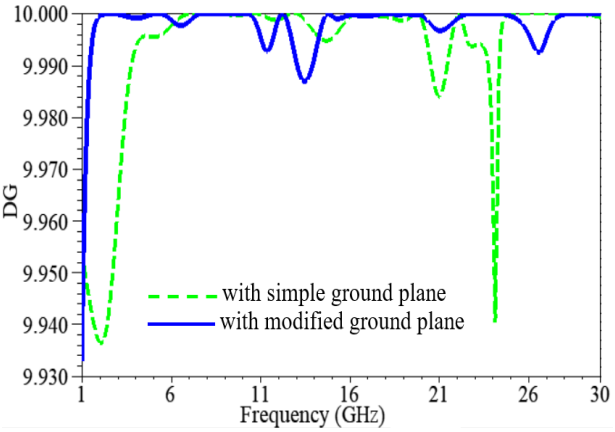

FIGURE 11(b). Diversity gain versus frequency plot of proposed MIMO hybrid antenna.

3) CCL

The CCL of the MIMO antenna is the maximum consistent data transmission rate without any loss in the communication channel. The CCL's ideal accepted minimum value is less than 0. 4bits/sec/Hz. A comparison of simulated and measured CCL versus the frequency plot of the proposed antenna has been illustrated in Fig. 12. CCL can be computed using equations (16) and (17). It can be corroborated that the value of CCL is much below the anticipated maximum value (< 0. 4bits/sec/Hz) at the required operative frequencies [73].

$$C_{loss} = -\log_{2}\left|\beta^{R}\right| \quad (16)$$

$$\beta^R = \begin{bmatrix} \beta_{11} & \beta_{12} \\ \beta_{21} & \beta_{22} \end{bmatrix} \quad (17)$$

Where

$$\beta_{11} = 1 - \left(|S_{11}|^2 + |S_{12}|^2 \right)$$

$$\beta_{22} = 1 - \left(|S_{22}|^2 + |S_{21}|^2 \right)$$

$$\beta_{12} = -\left(S_{11}^* S_{12} + S_{21}^* S_{22} \right)$$

$$\beta_{21} = -\left(S_{22}^* S_{21} + S_{12}^* S_{11} \right)$$

4) TARC

For the N-port antenna, the total active reflection coefficient (TARC) parameter is related to total occurrence power and total outward power. Preferably, it should be zero which means that complete power transported shall be acknowledged by the antenna. Therefore, it is demarcated as the relation of the square root of the total reflected power to the square root of total incident power [74]. The comprehensive TARC for N port antenna and for the instance of 2 port antenna can be computed from the (18) and (19) equations.

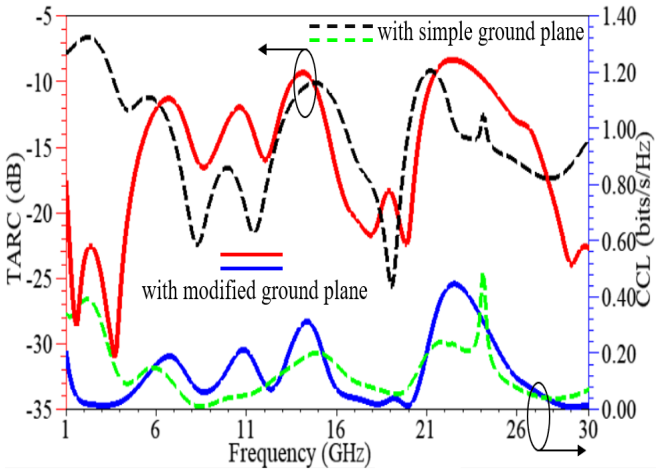

FIGURE 12. Total active reflection coefficient and channel capacity loss versus frequency plot of proposed MIMO hybrid antenna.

The comparison of simulated and measured TARC of proposed MIMO antenna has been deliberated in Fig. 12

$$\Gamma_a^t = \frac{\sqrt{\sum_{i=1}^{N} |b_i|^2}}{\sqrt{\sum_{i=1}^{N} |a_i|^2}} \quad (18)$$

$$\Gamma_a^t = \frac{\sqrt{\left(\left| \left(S_{11} + S_{12}^{e^{j\theta}} \right) \right|^2 + \left| \left(S_{21} + S_{22}^{e^{j\theta}} \right) \right|^2 \right)}}{\sqrt{2}} \quad (19)$$

Where, $b_i = [S].a_i.[S]$ is the scattering matrix

$[b] \rightarrow$ Scattering vector and $[a] \rightarrow$ excitation vector

C. SURFACE CUREENT DISTRIBUTION

The effects of the modified ground plane structure on the proposed antenna are analyzed with the help of surface current distribution plots at 2. 2, 8. 8, 12. 4, 16. 7, 20. 0, and 29. 2GHz frequency points as disclosed in Fig. 13. This analysis has been done by exciting port 1, to understand the mutual coupling reduction among the radiating elements and the ports. It can be understood from Fig. 13, that a strong current is being concentrated towards the modified ground plane along with the transmission line which helps in increasing the impedance bandwidth as well as reducing the mutual coupling between the ports. The stub-loaded ground plane helps to reduce the surface current to come closer to another MIMO antenna element.

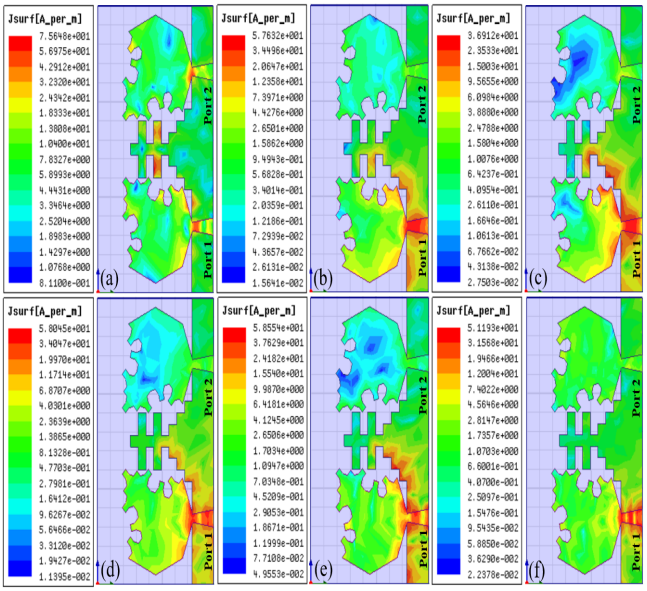

FIGURE 13. Surface current distribution of proposed MIMO antenna at (a) 2. 2, (b) 8. 8, (c) 12. 4, (d) 16. 7, (e) 20. 0 and (f) 29. 2GHz frequency points.

.

IV. *FABRICATED PROTOTYPE AND MEASURED RESULTS*

The proposed hybrid MIMO antenna is fabricated, and its prototype along with the testing setup is illustrated in Fig. 14. The measured *S*-parameters of the antenna are obtained by using the Rohde and Schwarz ZNB 40 VNA ranging from 100 KHz to 40GHz. Fig. 15, shows that reflection coefficient is below -10dB and the isolation is below -20dB for the complete frequency range from 1 to 30GHz.

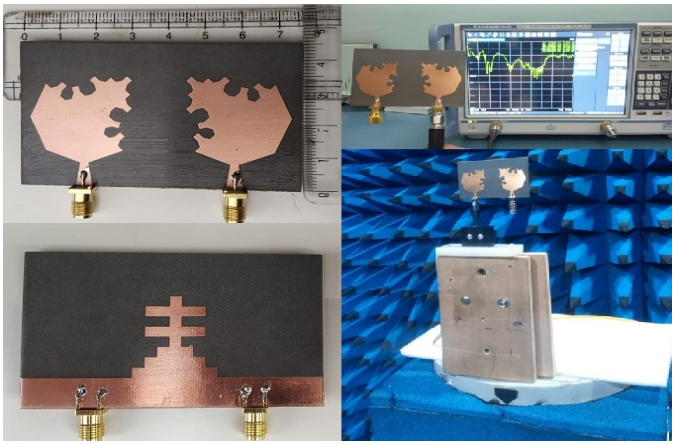

FIGURE 14. Front and rear view of fabricated prototype of proposed MIMO hybrid antenna along with testing setup.

This antenna also reveals the isolation between -20dB to -50dB for the entire frequency range from 1 to 30GHz for both the antennas (simulated and measured) with a reduction in the mutual coupling among the antenna elements.

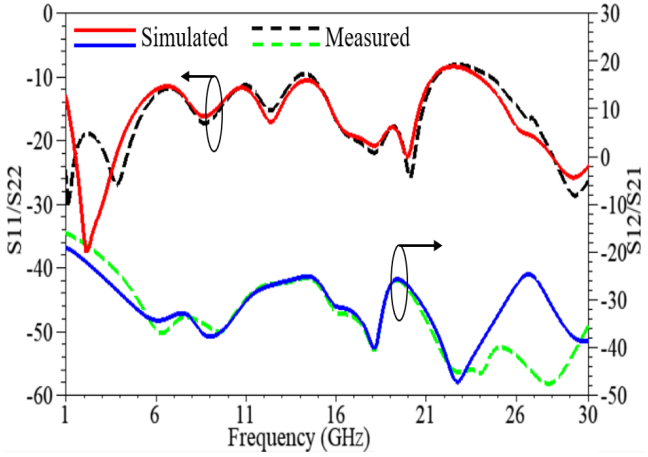

FIGURE 15. Comparison of simulated and measured S-parameter analysis of proposed MIMO hybrid antenna.

The proposed MIMO hybrid antenna exhibits wider impedance bandwidth characteristics along with the improvement in isolation characteristics as shown in Fig 15. So, the proposed MIMO hybrid antenna can be used for different wireless standards. The normalized 2D-radiation pattern in the E-plane (XZ-plane) and H-plane (YZ-plane) of the MIMO hybrid antenna are illustrated in Fig. 16 at distinct resonance frequency points such as 2. 2, 8. 8, 12. 4, 16. 7, 20. 0, and 29. 2GHz. The radiation patterns as shown in Fig. 16 are almost omnidirectional in both planes. The radiation pattern in E and H-plane at the higher frequency points is somewhat distorted and has increased due to the diversified short-wavelength electric current on the assembly of the antenna.

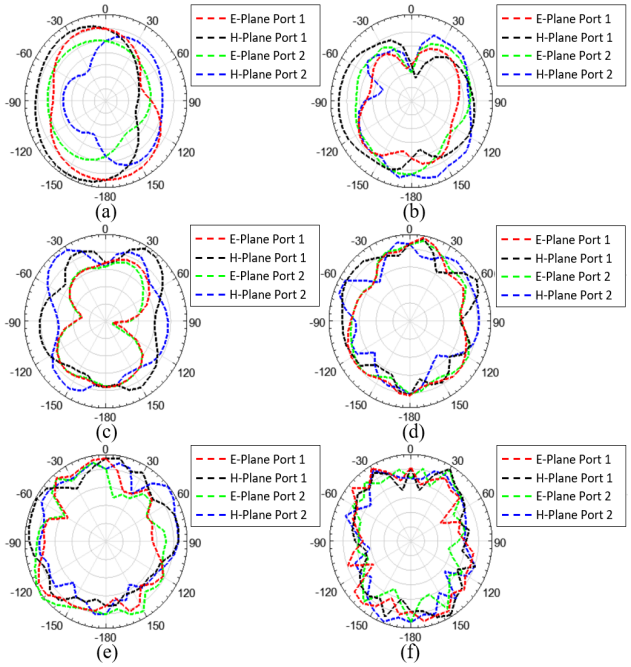

FIGURE 16. Normalized radiation patterns of proposed hybrid MIMO antenna at (a) 2. 2, (b) 8. 8, (c) 12. 4, (d) 16. 7, (e) 20. 0 and (f) 29. 2GHz in both E (XZ-plane) and H (YZ-plane).

The comparison plot of simulated and measured gain against frequency has been illustrated in Fig. 17. It can be observed that the gain is somewhat negative in the frequency range from 1 to 1. 5GHz. But after that, the gain exponentially rises to 8dBi as the operating frequency increases from 1. 5GHz to 8. 5GHz. Further, the gain is almost flat and varied between 4 to 7dBi in the frequency range from 8. 5GHz to 21. 1GHz. Similarly, the gain exponentially rises to 14dBi in the frequency range from 23. 9 to 25. 9GHz. The antenna becoming more directive at the particular frequency range is the main reason for the exponential rise in the value of gain.

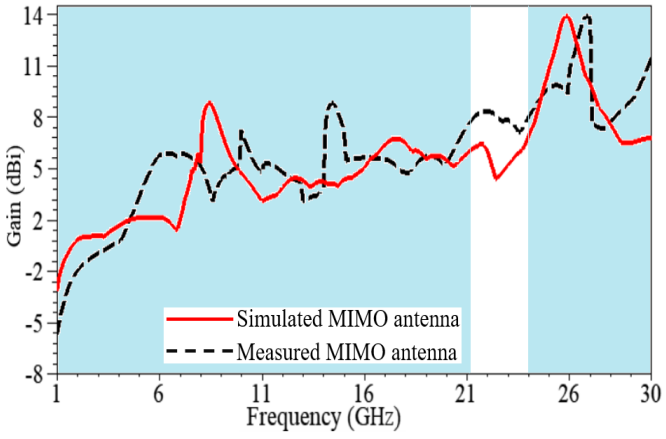

FIGURE 17. Peak realized gain versus frequency plot of proposed MIMO hybrid antenna

TABLE I. COMPARISON OF PROPOSED MIMO ANTENNA WITH EXISTING LITERATURE

Ref.	Dimension (mm^2)	Isolation (dB)	ECC	TARC	CCL	Ports
[75]	6000	20-40	<0. 04	---	---	2
[76]	7200	30	---	---	---	2
[77]	60000	25	0. 001	---	---	2
[78]	5640	20	<0. 04	---	---	2
[79]	5000	20-40	0. 0007	---	---	2
[80]	6000	<30	---	---	---	2
[81]	9600	<15	<0. 5	---	---	2
[82]	3500	<30	<0. 028	<-8	<0. 3	2
This work	3375	20-50	<0. 02	<-10	<0. 45	2

The proposed hybrid MIMO antenna is designed and considered for 5G and other wireless applications. Although existing literature embellishes several MIMO hybrid fractal antennas and MIMO fractal antennas yet proposed MIMO antenna is extremely competitive with the stated designs in terms of size, isolation, and impedance bandwidth. The proposed MIMO antenna is compact and also reveals competent performance. An all-inclusive parametric assessment of the proposed antenna with the available state-of-art literature is illustrated in Table I. for more clarity. Thus, it can be predicted from the table that the CCL, ECC, and TARC of the proposed MIMO antenna are at the required value, whereas, most of the stated designs are not assessed in terms of TARC and CCL. From, the above conversation, it is quite obvious that the proposed MIMO hybrid antenna can be used for distinct wireless applications.

V. CONCLUSION

A hybrid fractal shaped two-port MIMO antenna with stub loaded ground plane has been presented in this manuscript for 5G wireless applications. The performance of the proposed hybrid MIMO antenna with different ground planes has been compared and it found that the antenna with a modified ground plane is better in terms of improved bandwidth, reflection coefficient, and reduction in mutual coupling. The proposed MIMO antenna reveals the wider impedance bandwidth of 20. 4GHz (1. 0 to 21. 4GHz) and 6. 10GHz (23. 9 to 30GHz) with a fractional bandwidth of 182. 14% and 22. 63% respectively. Diversity performance parameters such as CCL, DG, ECC, and TARC are within reasonable limits. The proposed hybrid fractal MIMO antenna is a proficient candidate for 5G 3. 5GHz band (3. 4 – 3. 6GHz), 5G NR (New Radio) frequency bands (3. 3 – 5. 0GHz), LTE band 46 (5. 15 – 5. 925GHz), EU (European Union) 5G frequency band (5. 9 – 6. 4GHz), UWB applications (3. 1 – 10. 6GHz), 5G 26GHz frequency band, and the other applications in the obtained operational frequency range (1 – 21. 4GHz and 23. 9 – 30GHz).

ACKNOWLEDGMENT

The authors would like to thank Rogers Corporation for providing the material RT/duroid 5880 and also thanks to Ramaiah Institute of Technology, Bangalore for providing the facility to test the fabricated prototype.

REFERENCES

[1] Li Z, Du Z, Gong K, "A dual-slot diversity antenna with isolation enhancement using parasitic elements for mobile handsets", *Proceedings Asia Pacific Microwave Conference*, pp. 1821–24, 2009.

[2] H. Abdi, J. Nourinia and C. Ghobadi, "Compact CPW-Fed Antenna for Enhanced UWB applications", *Advanced Electromagnetics*, vol. 10, no. 1, pp. 15-20, January 2021.

[3] C. C. Hsu, K. H. Lin, H. L. Su, H. H. Lin and C. Y. Wu, "Design of MIMO antennas with strong isolation for portable applications, " *Antennas and Propagation Society International Symposium*, IEEE, pp. 1-4, 2009.

[4] A. Ramachandran, S. Mathew, V. Rajan and V. Kesavath, "A Compact Triband Quad-Element MIMO Antenna Using SRR Ring for High Isolation, " *IEEE Antennas and Wireless Propagation Letters*, vol. 16, pp. 1409-1412, 2017.

[5] J. Y. Lee, S. H. Kim and J. H. Jang, "Reduction of Mutual Coupling in Planar Multiple Antenna by Using 1-D EBG and SRR Structures, " *IEEE Transactions on Antennas and Propagation*, vol. 63, no. 9, pp. 4194-4198, Sept. 2015.

[6] Q. Li, A. P. Feresidis, M. Mavridou and P. S. Hall, "Miniaturized Double-Layer EBG Structures for Broadband Mutual Coupling Reduction Between UWB Monopoles, " *IEEE Transactions on Antennas and Propagation*, vol. 63, no. 3, pp. 1168-1171, March 2015.

[7] M. J. Al-Hasan, T. A. Denidni and A. R. Sebak, "Millimeter-Wave Compact EBG Structure for Mutual Coupling Reduction Applications, " *IEEE Transactions on Antennas and Propagation*, vol. 63, no. 2, pp. 823-828, Feb. 2015.

[8] Deng, Jing & Wang, Zhu & Li, Jin & Guo, "A dual-band MIMO antenna decoupled by a meandering line resonator for WLAN applications," *Microwave and Optical Technology Letters*, vol. 60, pp. 759-765, 2018.

[9] Talha, M. Babu, K., & Aldhaheri, "Design of a compact MIMO antenna system with reduced mutual coupling", International Journal of Microwave and Wireless Technologies, pp. 117-124, 2016.

[10] A. M. M. A. Allam and A. M. G. Hemdan, "Novel DGS shape for mutual coupling reduction, " *German Microwave Conference (GeMiC)*, pp. 278-281, 2016.

[11] S. M Refaat, A. Abdelaziz and Ehab K. I. Hamad, "Tri-Band Slot-Loaded Microstrip Antenna for Internet of Thing Applications", *Advanced Electromagnetics*, vol. 10, pp. 21-28, March. 2021.

[12] M. Harbadji, A. Boufrioua and T. A. Denidni, "Triple band Compact Fractal Antenna with Defected Ground Plane for Bluetooth, WiMAX, and WLAN Applications", *Advanced Electromagnetics*, vol. 7, pp. 26-30, Sept. 2018.

[13] R. Sahoo and D. Vakula, "A Cylindrical Wideband Conformal Fractal Antenna for GPS Application", *AdvancedElectromagnetics*, vol. 6, pp. 64-68, Oct. 2017.

[14] P. C. Nirmal, A. Nandgaonkar, S. L. Nalbalwar, and R. K. Gupta, "A Compact Dual Band MIMO Antenna with Improved Isolation for Wi-MAX and WLAN Applications, " *Progress In Electromagnetics Research M*, vol. 68, pp. 69-77, 2018.

[15] A. Iqbal, O. A. Saraereh, A. W. Ahmad and S. Bashir, "Mutual Coupling Reduction Using F-Shaped Stubs in UWB-MIMO Antenna, " *IEEE Access*, vol. 6, pp. 2755-2759, 2018.
[16] J. Y. Lee, S. H. Kim and J. H. Jang, "Reduction of Mutual Coupling in Planar Multiple Antenna by Using 1-D EBG and SRR Structures, " *IEEE Transactions on Antennas and Propagation*, vol. 63, no. 9, pp. 4194-4198, Sept. 2015.
[17] J. Sun, H. Fang, P. Lin and C. Chuang, "Triple-Band MIMO Antenna for Mobile Wireless Applications, " *IEEE Antennas and Wireless Propagation Letters*, vol. 15, pp. 500-503, 2016.
[18] Wu, Di & Cheung, William & Li, Qinlong & Yuk, "Decoupling Using Diamond-shaped Patterned Ground Resonator for Small MIMO Antennas", *IET Microwaves, Antennas & Propagation*, pp. 177–83, 2016.
[19] G. Pal and N. Sharma, " Novel Design of Fractal Antenna using Giuseppe Peano Geometry for Wireless Applications", *International Journal of Computer Applications*, pp. 29-32, 2016.
[20] N. Sharma, G. P. Singh and V. Sharma, "Miniaturization of fractal antenna using novel Giuseppe peano geometry for wireless applications, " *IEEE 1st International Conference on Power Electronics, Intelligent Control and Energy Systems (ICPEICES)*, pp. 1-4, 2016.
[21] P. Kumar and S. Kaushik, "Design and Analysis of Ultra Wide Band Giuseppe Peano Fractal Antenna at Different Height Level of Substrate", *International Journal of Engineering Trends and Technology (IJETT)*, vol. 61, pp. 117-120, 2018.
[22] V. Radonic, K. Palmer, G. Stojanvoic and V. C. Bengin, "Flexible Sierpinski Carpet Fractal Antenna on a Hilbert Slot Patterned Ground, " *International Journal of Antennas and Propagation, pp. 1-7, 2012.*
[23] P. Bhutani, S. Sagar, A. Kumar, "Performance Analysis of Sierpinski Carpet Fractal Antenna for Wireless Communication Applications of Computing", *Automation and Wireless Systems in Electrical Engineering,* vol. 553, pp. 749-58, 2019.
[24] A. Gehani, P. Agnihotri, and D. A. Pujara, "Analysis and Synthesis of Multiband Sierpinski Carpet Fractal Antenna Using Hybrid Neuro-Fuzzy Model", *Progress In Electromagnetics Research Letters,* vol. 68, pp. 59-65, 2017.
[25] S. Datta**,** K. Kar**,** M. Pal and R. Ghatak**,** "Fractal Shaped Antenna based tri-band Energy Harvester", *AdvancedElectromagnetics*, vol. 06, *pp.* 22–26, 2017.
[26] G. Liu, J. Gu, Z. Gao and M. Xu, "Wideband printed slot antenna using Koch fractal metasurface structure", *International Journal of RF and Microwave Computer Aided Engineering*, pp. 1-6, 2016.
[27] C. Elavarasi and T. Shanmuganantham, " Multiband SRR loaded Koch star fractal antenna", *Alexandria Engineering Journal*, vol. 57, pp 1549-1555, 2018.
[28] A. A. Omar, "Design of ultrawideband coplanar waveguide-fed koch-fractal triangular antenna", *International Journal of RF and Microwave Computer Aided Engineering*, pp. 1-8, 2012.
[29] J. Salini, S. Natarajamani andS. M. Vaitheeswaran, "Minkowski fractal circularly polarized planar antenna for GPS application", *Procedia Computer Science,* vol. 143, pp. 66-73, 2018.
[30] D. Sur, A. Sharma, R. K. Gangwar, N. K. Sahu, "A novel wideband Minkowski fractal antenna with assistance of triangular dielectric resonator elements", *International Journal of RF and Microwave Computer Aided Engineering*, pp. 1-8, 2018.
[31] R. Ataeiseresht, C Ghobadi and J. Nourinia, "A Novel Analysis of Minkowski Fractal Microstrip Patch Antenna", *Journal of Electromagnetic Waves and App*, pp. 1115-27, 2006.
[32] T. Olawoye and P. Kumar, "A High Gain Antenna with DGS for Sub-6 GHz 5G Communications,"*Advanced Electromagnetics*, vol. 11, pp. 41-50, March. 2022
[33] P. Wang, G. J. Wen, Y. J. Huang and Y. H. Sun, "Compact meander T-shaped monopole antenna for dual-band WLAN applications", *International Journal of RF and Microwave Computer Aided Engineering,* pp. 1-7, 2012.
[34] H. Shawkey and D. Elsheakh, "Multiband Dual-Meander Line Antenna for Body-Centric Networks", *Biomedical Applications by Using UMC 180 nm,* Electronics, pp. 1-11, 2020.
[35] M. Singh, N. Kumar, S. Dwari and P. Kala, "Metamaterial-inspired miniaturized antenna loaded with IDC and meander line inductor using partial ground plane", *International Journal of RF and Microwave Computer-Aided Engineering,* pp. 1-10, 2019.
[36] M. Palandoken and C. Gocen, "A modified Hilbert fractal resonator based rectenna design for GSM900 band RF energy harvesting applications", *International Journal of RF and Microwave Computer Aided Engineering*, pp. 1-8, 2019.
[37] K. J. Vinoy, K. A. Jose, V. K. Varadan and V. V. Varadan, "Hilbert curve fractal antenna: A small resonant antenna for VHF/UHF applications", *Microwave and Optical Technology Letters,* pp. 2015-19, 2001.
[38] A. Kumar and A. P. S. Pharwaha, "Development of a Modified Hilbert Curve Fractal Antenna for Multiband Applications", *IETE Journal of Research*, 2020.
[39] N. Kaur, J. Singh, &M. Kumar, "Hexagonal Ring Shaped Dual Band Antenna Using Staircase Fractal Geometry For Wireless Applications", *Wireless Personal Communication,* pp. 2067–2078, 2020.
[40] N. Kaur, J. Singh and M. Kumar, "SRR and Rectangular stubs loaded Novel Fractal antenna realization for Multiband Wireless applications", *Wireless Personal Communication,* pp. 1-19, 2021.
[41] G. Bharti and J. S. Sivia, "A design of multiband Nested Square shaped Ring Fractal antenna with circular ring elements for wireless applications", *Progress In Electromagnetic Research*, vol. 108, pp. 115-125.
[42] R. Sahoo and D. Vakula, "A Cylindrical Wideband Conformal Fractal Antenna for GPS Application", *Electromagnetics*, vol. 06, pp. 64-69, 2017.
[43] V. V Reddy, "Broadband Koch Fractal Boundary Printed Slot Antenna for ISM Band Applications", *Advanced Electromagnetics*, vol. 07, pp. 31-36, 2018.
[44] S. S. Sran and J. S. Sivia, "ANN and IFS based wearable hybrid fractal antenna with DGS for S, C and X band application", *AEU- Int Journal of Electronics and Communication*, vol. 127, 2020.
[45] M. Kaur and J. S. Sivia, "ANN and FA based design of Hybrid Fractal antenna for ISM band applications", *Progress In Electromagnetic Research,* vol. 98, pp. 127-140.
[46] A. T Abed and A. M Jawad, "Compact size MIMO Amer fractal slot antenna for 3G, LTE(4G), WLAN, WiMAX, ISM and 5G Communications", *IEEE Access*, vol. 7, pp. 125542-51, 2019.
[47] A. T Abed, "Novel sunflower MIMO fractal antenna with low mutual coupling and dual wide operating bands", *International Journal of Microwave and Wireless Technology*, pp. 323-31, 2019.
[48] R. Avula, M. Rangarao and Y Kumari, "Fractal Ultra-Wideband antenna for 5G applications", *International Journal of Recent Technology and Engineering*, vol. 07, pp. 215-18, 2019.
[49] K. Venkatrao, S. H. Priya, R. Raghavendra, M. N. Kiran and D. Sumanth, "Multi-band Minkowski fractal antenna for 5G applications", *International Journal of Recent Technology and Engineering,* vol. 8, pp. 3525-30, 2020.
[50] S. Gundala, V. S. Baba, A. Vijaya and S. Machanna, "Compact high gain hexagonal antenna for 5G applications", *IEEE International Conference on Advanced Networks and Telecommunication systems*, pp. 1-7, 2019.
[51] G. V Ramanaiah, N. Rajyalakshmi, V. S. Tejaswini, M. D. Pasha, V. D. N. V. S Manoj Kumar, "Ultra-Wide band fractal antenna for 5G applications", *International Journal of Research in Electronics and Computer Engineering,* pp. 1058-61, 2019.
[52] G. N Jyoti and S. Nelaturi, "Design and experimental verification of fractal-based MIMO antenna for lower sub-6-GHz 5G applications", *AEU- International Journal of Electronics and Communication*, vol. 137, 2021.
[53] S. Patil and V. Rohokale, "Multiband smart fractal antenna design for covereged 5G wireless networks", *International Conference on* Pervasive Computing (ICPC)*,* pp. 1-5, 2015.
[54] G. P. Mohan, "Design and development of fractal microstrip patch antenna for 5G communication", *Advances in Wireless and Mobile Communication*, vol. 10, pp. 13-25, 2017.
[55] B. P. A. Mahatmanto, C. Apriono, F. Y. Zulkifli, E. T. Rahardjo, "Hexagonal triangular fractal antenna with tapered feedline and reflector for 5G and UWB applications", *IEEE Conference on Antenna Measurementand Applications(CAMA)*, pp. 1-4, 2019.

[56] A. Sabban, "Wearable systems and antennas technologies for 5G", 1st ed., *IOT and medical systems. Engineering and Technology*, Albert Sabban, 2020.

[57] Md. Ashfaq, Zahid, H. Shadman and F. B. Faruquee, "Wideband Minkowski fractal antenna using complementary split ring resonator in modified ground plane for 5G wireless communications", *Engineering Reports*, pp. 1-22, 2021.

[58] K. Shet, K. GS and H. S. Suraj, "A wideband probe-fed low-cost mm wave fractal antenna array for 5G", *International Conference on Advances in Physical Science and Materials*, pp. 1-9, 2020.

[59] P. K. Choudhury and A. E. Nasr, "Massive MIMO toward 5G", *Journal of Electromagnetic waves and Applications*, vol. 34, pp. 1091-94, 2020.

[60] R. Chataut, R. Akl, "Massive MIMO systems for 5G and beyond Networks – Overview, recent trends, challenges, and future research direction", *Sensors* 2020; 20(10):2753. DOI: 10. 3390/s20102753

[61] A. K. Sohi and A. Kaur, "UWB aperture coupled circular fractal MIMO antenna with a complementary rectangular spiral defected ground structure (DGS) for 4G/WLAN/radar/satellite/international space station (ISS) communication systems", *Journal of Electromagnetic waves and Applications*, pp. 2317-38, 2020.

[62] K. H Sayidmarie, N. J McEwan, P. S Excell, R. A Abd-Alhameed, and C. H See, "Antenna for emerging 5G systems", *International Journal of Antenna and Propagation*, pp. 1-3, 2019.

[63] K. Maruta and F. Falcone, "Massive MIMO systems: Present and Future", Electronics 2020, DOI:10. 3390/electronics9030385.

[64] M. S Khan, A. Iftikhar, R. M Shubair, A. D Capobianco, B. D Braaten and E. Dimitris, "Ultra-wideband antenna with MIMO diversity for 5G wireless communication", *Electrical Engineering and System. Signal Processing (eess. SP) Applied Physics (physics. app-ph)*, 2020.

[65] A. Abboud, J. P Cances, V. Meghdadi and A. Jaber, "Smart Massive MIMO: An infrastructure towards 5th generation smart cities network", *Computer Science, Networking and Internet Architecture (cs. NI)*, 2016.

[66] Usha Devi Y, M. TP Boddapati, T. A. Kumar, S. K. C. K and P. Pardhasaradhi, "Conformal printed MIMO antenna with DGS for millimeter wavecommunication applications", *International Journal of Electronics Letters*, vol. 8, pp. 329-43, 2020.

[67] M. Benzaghta, K. M. Rabie", MassiveMIMO systems for 5G: A systematic mapping study on antenna design challenges and channel estimation open issues", *IET Institution of Engineering and Technology*, 2021.

[68] N. Sharma, S. S Bhatia and V. Sharma, "Peano-Gosper, Koch and Minkowski fractal curves-based novel hybrid antenna using modified partial ground plane for multi-standard wireless applications", *Journal Electromagnetic Waves Applications*, vol. 35, 2021.

[69] N. Sharma, V. Sharma, S. S Bhatia, "A novel hybrid fractal antenna for wireless applications", *Progress In Electromagnetic Research M,* vol. 73, pp. 25-35, 2018.

[70] N. Sharma and S. S Bhatia, "Split ring resonator based multiband hybrid fractal antennas for wireless applications", *International Journal Electronics&Communications(AEU)*, vol. 93, pp. 39-52, 2018.

[71] K. V Babu and B. Anuradha, "Design of multi-band Minkowski MIMO antenna to reduce the mutual coupling", *Journal of King Saud University - Engineering Sciences,* vol. 32, pp. 51-57, January 2020.

[72] A. Dkiouak, A. Zakriti, M. Elouahabi, H. Elftouh, A. Mchbal, "Design of CPW-fed MIMO for ultra-wideband communications", *Procedia Manufacturing*, vol. 46, pp. 782-87, 2020.

[73] R. Gurjar, D. K. Upadhyay, B. K. Kanaujia and A. Kumar, "A compact modified Sierpinski carpet fractal UWB MIMO antenna with square-shaped funnel like ground stub", *AEU-International Journal of Electronics & Communication,* vol. 117, 2020.

[74] AW. M. Saadh, K. Ashwath and P. Ramaswamy, "A uniquely shaped MIMO antenna on FR4 material to enhance isolation and bandwidth for wireless applications", *AEU-International Journal of Electronics & Communication*, vol. 123, 2020.

[75] S. Roy and U. Chakraborthy, "Mutual coupling reduction in a multi-band MIMO antenna using meta-inspired decoupling network", *Wireless Personal Communication,* vol. 114, pp. 3231-46, 2020.

[76] C. Pan and T. J Cui, "Broadband decoupling network for dual-band microstrip patch antennas", *IEEE Transactions on Antennas and Propagation*, vol. 65, pp. 5595-5598, Dec. 2017.

[77] Z. H Jiang, "A compact triple-band antenna with a notched ultra-wideband and its MIMO array", *IEEE Transactions on Antennas and Propagation*, vol. 66, pp. 7021-31, 2018.

[78] X. Liu, Y. Wu, Z. Zhuang, W. Wang and Y. Liu, "A dual-band patch antenna for pattern diversity application", *IEEE Access*, vol. 6, pp. 51986-51993, 2018.

[79] X. Zhao, S. P Yeo and L. C Ong, "Decoupling of inverted-F antennas with high-order modes of ground plane for 5G mobile MIMO platform", *IEEE Transactions on Antennas and Propagation*, vol. 66, pp. 4485-95, 2018.

[80] Y. Yang, Q. Chu and C. Mao, "Multiband MIMO antenna for GSM, DCS, and LTE indoor applications", *IEEE Antennas and Wireless Propagation Letters*, vol. 15, pp. 1573-76, 2016.

[81] S. Wang and Z. Du, "Decoupled dual-antenna system using crossed neutralization lines for LTE/WWAN smartphone applications", *IEEE Antennas and wireless Propagation Letters,* vol. 14, pp. 523-26, 2015.

[82] R. Saleem, M. Bilal, H. T Chattha, S. U Rehman, A. Mushtaq and M. F Shafique, "An FSS based multiband MIMO system incorporating 3D antennas for WLAN/WiMAX/5G cellular and 5G Wi-fi applications", *IEEE Access,* vol. 07, pp. 144732-740.